Surface and downhole electrodes in electrical resistivity tomography

Marco A. S. Vilar, Andrea Ustra, Carlos A. Mendonça

Department of Geophysics, IAG/USP

Abstract

Electrical resistivity tomography (ERT) is a mature geophysical method serving as a tool in many nearsurface investigations. Modern investigations combine electrodes at surface with electrodes within boreholes in order to increase data sensitivity to deeper levels. This helps the investigation of places with constructed areas where open space to deploy electrodes is short. We present a test site experimentation in which the investigation of deeper levels was prevented by the presence of a conductive layer and limitations to deploy lengthier arrays. By supplementing surface electrodes with few electrodes down hole, a resistivity section better matching well-logging and geological data was obtained. Our results illustrate the importance of using lengthier profiles at surface even when electrodes in wells are used, as well as the importance in data inversion of using a reference model based on local geology.

Introduction

Standard techniques for site characterization are based on direct probing (e.g., cone penetration or standard penetration test) applied along profiles or regular grids where future pit work is developed. However, even when closed spaced, subtle variations between adjacent probing points may be missed. Combination of direct probing with geophysical investigation is a way to complement detailed information from coring and drill cuts, with lateral coverage provided by geophysical images. An effective approach consists in installing a set of electrodes in the interior of wells to perform resistivity imaging (ERT- Earth Resistivity Tomography). The installation of electrodes in boreholes to complement surface arrays has found many applications (Loke et al., 2013); for example, to monitor carbon dioxide sequestration (Bergman et al., 2012); to assess rock mass integrity in the roof of tunnels (Tsokas et al., 2014); to outline pockets of free-gas phases (methane and carbon dioxide) in organic sediments of a buried wetland (Mendonça et al., 2015). The installation of permanent electrodes in deeper levels can monitor potentially hazardous industrial areas (Pidlisecky et al, 2006).

Electrodes along parallel holes can investigate tunneling fronts (Danielsen and Dahlin, 2010) and monitor the remediation of contaminated sites (Power et al., 2015).

Basic assumption in combining surface and borehole electrodes is that model sensitivity to available data set is enhanced when electrodes are collocated closer to the domain intended to be imaged. We present a case study showing the usefulness of surface-down hole ERT surveys at a test site in Sao Paulo, Brazil. Our main attempt is to understand in what conditions a reliable resistivity model for the subsurface can be obtained if additional electrodes were collocated within a borehole. This exploratory scenario is particularly important for further investigations in the São Paulo Basin, where many subsurface engineering operations are developed. In general, these results may give some guidance to ERT investigations using combinations of surface and borehole electrodes.

Theoretical Aspects

The subsurface in ERT is represented by a set of m cells of known dimension and size but unknown resistivity, organized as a m-dimensional vector, $\mathbf{p}$, whose entries p_i, $i = 1, \cdots, m$ denote cell resistivity of the i-th cells. For a data set, $\mathbf{d}_0$, for n apparent resistivity measurements, a functional

$$Q(\mathbf{p}) = \|\mathbf{d}_0 - \mathbf{d}_c(\mathbf{p})\|_q + \mu \|\mathbf{p} - \mathbf{p}_0\|_q \qquad (1)$$

is minimized to provide a resistivity model either allowing data fitting (first parcel in equation 1) as well as a minimum departure of this model from a reference model, $\mathbf{p}_0$ (second parcel). Term $\mathbf{d}_c \equiv \mathbf{d}_c(\mathbf{p})$ stands for model response evaluated from model $\mathbf{p}$, and μ is an regularizing parameter balancing data fitting quality against model departure from $\mathbf{p}_0$. Term $\|\cdot\|_q$ for $q \geq 1$ assigns a generalized q-norm; $q = 2$ standing for the Euclidean or L-2 norm and $q = 1$ for the absolute or L-1 norm. When applied to the model parameter, the L-1 norm provides what is termed as "flat" solutions that favor models with contrasting resistivity between rather uniform resistivity domains.

Mathematical operations to evaluate model response, $\mathbf{d}_c(\mathbf{p})$, involve the solution of a partial differential equation

$$\nabla \cdot (\sigma \nabla \varphi) = -I\big(\delta(\mathbf{r} - \mathbf{r}_+) - \delta(\mathbf{r} - \mathbf{r}_-)\big) \qquad (2)$$

under appropriated boundary conditions (Pidlisecky et. al, 2007; Karaoulis et al. 2013) to determine the electric potential φ in response to bipolar current with intensity, I, and plus and minus terminations at positions $\mathbf{r}_+$ and $\mathbf{r}_-$.

Numerical solutions for equation 2, to evaluate $\mathbf{d}_c(\mathbf{p})$ formally is written as (Pidlisecky et al., 2006)

$$\mathbf{d}_c(\mathbf{p}) = \mathbf{KSA}^{-1}\mathbf{q} \qquad (3)$$

in which $\mathbf{A} \equiv \mathbf{DPG}$, where $\mathbf{D}$ and $\mathbf{G}$ are matrices representing second order finite-difference for divergence and gradient operators, respectively, and $\mathbf{P}$ a diagonal matrix with elements equal such that j-th entry represents the resistivity of the j-th cell, $\mathbf{S}$ is a sampling matrix pinking out the difference potentials at sampling points (Pidlisecky et al., 2006) and $\mathbf{K}$ a diagonal matrix with geometrical factors accounting for the distances between current and potential electrodes.

To minimize functional in equation 2, the expressions under the norm parameter are linearized as

$$\mathbf{p}_{k+1} = \mathbf{p}_k + \Delta\mathbf{p}_k \qquad (4)$$

starting with $k = 1$ and updated in steps $\Delta\mathbf{p}_k$ according to

$$\Delta\mathbf{p}_k = -(\mathbf{J}^T\mathbf{J} + \mu\mathbf{I})^{-1}[\mathbf{J}^T(\mathbf{KSA}^{-1}\mathbf{q} - \mathbf{d}_0) - \mu(\mathbf{p}_k - \mathbf{p}_0)] \quad (5)$$

where $\mathbf{J}$ is the Jacobian or sensitivity matrix whose entry i,j is given by derivative $\partial d_{c,i}/\partial p_j$ (i-th data derivative with respect to j-th model parameter) and superscript, T, denoting matrix transposition, $\mathbf{I}$ is the identity matrix. Model sensitivity, S_j for the j-th cell of the model can be evaluated as

$$S_j^2 = \sum_{i=1}^{n}\left(\frac{\partial d_{c,i}}{\partial p_j}\right)^2 \qquad (6)$$

which expresses the Euclidean norm of i-th row of sensitivity matrix $\mathbf{J}$. Optimized formulations are necessary to compute the sensitivity matrix and operations in which it is involved (Haber et al., 2000).

Figure 1 illustrates the operations involved in the inversion of resistivity data and geological interpretation of the inverted resistivity section. The elements feeding data inversion are the set of measured data, a sort of a priori information about the model parameters (e.g., flatness, smoothness, and positivity) and a reference model for iterative updating as given by equations 4 and 5. The quality of the data fitting can be assessed by a norm (L-1 or L-2), residual root-mean-squares (RMS), or displayed visually by means of a cross-plot graphic of the measured and evaluated from the model data. The interpretation of the resistivity model requires a side-by-side check of model sensitivity evaluated (equation 6) for each cell of the model.   Portions of the resistivity section with low sensitivity should not be interpreted in terms of geology since they are not conditioned by information provided by the data, but instead most conditioned by the initial model serving as input.
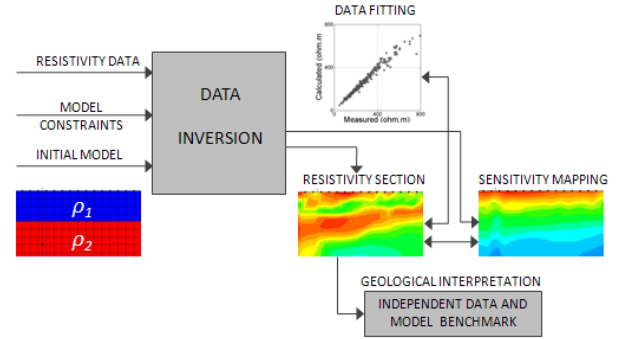

Figure 1: Simplified flowchart of resistivity data inversion and resistivity section interpretation. In this case, a reference layered model with resistivities of ρ_1 and ρ_2. Main outputs: resistivity section, cross plot to evaluate data fitting, model sensitivity map outlining regions better resolved by available data. Low sensitivity regions are not uniquely retrieved from data, and as such, rely on information provided by the reference model. Independent geological information from wells is benchmarks the resistivity section.

Materials and Methods

Test site geology
The test site is located at the campus of the University of São Paulo, in São Paulo, Brazil. The area is part of the SGTS -Shallow Geophysical Test Site of IAG-USP, used by the Department of Geophysics of the IAG/USP for research and teaching purposes. Several geophysical investigations have been conducted at this site, to map sediments and detect the basement topography (Porsani et al., 2004). Figures 1a) and 1b) with well logging and geological information show a section with an anthropogenic layer at the top, Cenozoic sediments of the São Paulo Basin in the middle and the crystalline basement at the bottom. The upper portion of the Cenozoic sediments is constituted by alternations of silt-argillite and silt-sandstones layers, with resistivity of about 100 ohm.m and 700 ohm, respectively. Its lower portion is composed by an uniform clay layer, with resistivity increasing upward from 30 ohm.m to about 100 ohm.m. The basement at 53 m depth is composed by granite-gneisses of the Pre-Cambrian age. Weathering in the basement upper portion (53 to 62 m) lower its resistivity with respect to the underneath fresh rocks (3×10^3ohm.m) but still contrasting with above clayey sediment.

For ERT with surface electrodes, the low resistivity of the basal layer prevents the investigation of deeper levels. The amplitude of the electric potential for large arrays drops to noise levels for common offsets (200-300 m) and current intensity (~1 A) used in common near surface investigations, preventing the investigation levels reaching the basement.
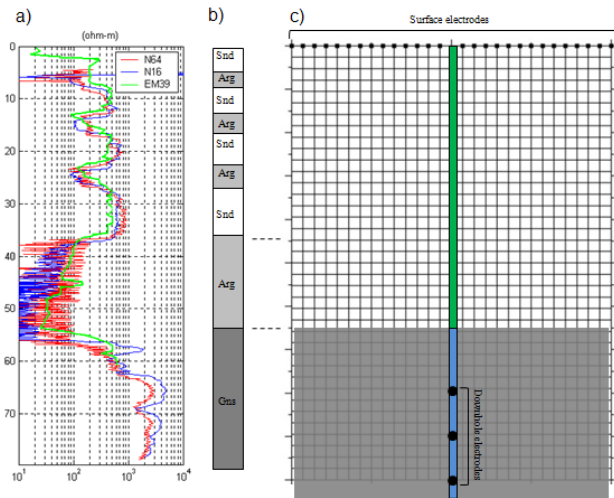
Figure 2: a) Resistivity well-logging, long and short normal (red and blue) and induction log (green) with EM-39/Geonics; b) rock formations crossed by the well; c) mesh for resistivity inversion with position of electrodes at surface and down hole (full black circles), with representation of a two-layer model (upper white and lower gray cells). The sediments are composed sandstones (Snd) and argillites (Arg). The well was cased at the section with sediments (green), and open at the basement where electrodes were lowered.

Earth resistivity imaging

To evaluate the feasibility to investigate deeper levels with limited surface space, we used a combination of surface and downhole electrode arrays composed by a set of 28 electrodes at the ground surface and 3 electrodes lowered downhole. Since the testing well was cased all the way in the sedimentary column, the electrodes down hole were distributed along the interval with the crystalline basement. Figure 1c) shows a sketch of the survey line, with electrodes lying at the surface (surface electrodes) and inside the borehole (down hole electrodes). Intending a regular distribution, the electrodes in the borehole were positioned at depths of 60, 68 and 76 m. Once the electrodes were fixed in the borehole, two data acquisition rounds were conducted, with surface electrodes spaced by 2 m and 4 m, corresponding to profile lengths of 54 m and 108 m, respectively. Measurements were taken with a multi-electrode resistivimeter (StingR1IP/AGIUSA), using a multi-channel cable connecting the electrodes to a switchbox. The resistivimeter was programmed to commute electrode pairs according dipole-dipole and wenner arrays resulting a set of 460 readings.

Data-bases for profiles with 54 and 108 m were inverted separately with the software EarthImager 2D (AGIUSA), by minimizing the L-2 for data residuals and model parameters. Input data sets were filtered to remove noisy reading, discarding points with repetition errors higher than 3%. After a preliminary data fitting with low μ (~0.001) data points providing higher than 5-6% misfit were discarded from next round of data inversion. Rationale here was not to fit a subset of outlier points, at the expenses to obtain distorted resistivity models. By satisfying a larger subset of the data (~90%) the effects from noisy and outlier points were minimized and

distortions on the resistivity models minored. Since different output solutions were achieved from changing the input reference models, the corresponding sensitivity maps also were different. A basic criterion to account for the reliability of the inverted resistivity section is that the basement topography as inferred from refraction and reflection seismic (Porsani et al., 2004) is rather flat, practically horizontal at the window investigated by the resistivity sections.

The next step consisted in determining a proper value for the regularizing parameter μ, since a lower value tends to ignore (or to null) the constraints upon the model parameters and a higher one degrades data fitting, not honoring the data sets within experimental margin of error. We tune this parameter by interactively determining the residuals L-2 norm as a function of μ from 0.001 to 1000, as approximately distributed into a log scale. A proper value for μ was determined as that limiting value up of which data fitting residuals abruptly increases. This inflection point (100 in our case) assigns the maximum value for μ, above which data fitting becomes arbitrarily degraded by the interpreter choice.

Finally, for each data set the inversion procedure was applied twice, one by feeding as reference model an homogeneous half-space, the other by feeding it with a two-layer model, correctly assigning the depth of the basement identified by the well. Output models in terms of candidate solutions were analyzed with bases on local geology. The candidate solution compatible with general properties of local geology were elected as the best model (or best subsurface representation) and subjected to geological interpretation.

Results

Results for profile lengths of 54 m and 108 m are presented in Figures 3 and 4, respectively. Since different output solutions were achieved from changing the input reference models, the inverted sections obtained using the homogeneous earth and two layers models are shown separately, as well as the corresponding sensitivity maps also were different. A basic criterion to account for the reliability of the inverted resistivity section is that the basement topography as inferred from refraction and reflection seismic is horizontal.

The resistivity images for profile with 54 m (Figures 3c and d) do not clearly identify the conductive layer over the basement. In addition, a spurious resistive feature appears connecting the resistive basement with the resistive sediments of the upper sequence of the sediments. This feature is caused by the lack of sensitivity in the intermediary depths of the section (Figures 3e and f). As a rule, the sensitivity is higher near the electrodes, letting a sensitivity gap in the intermediary levels.
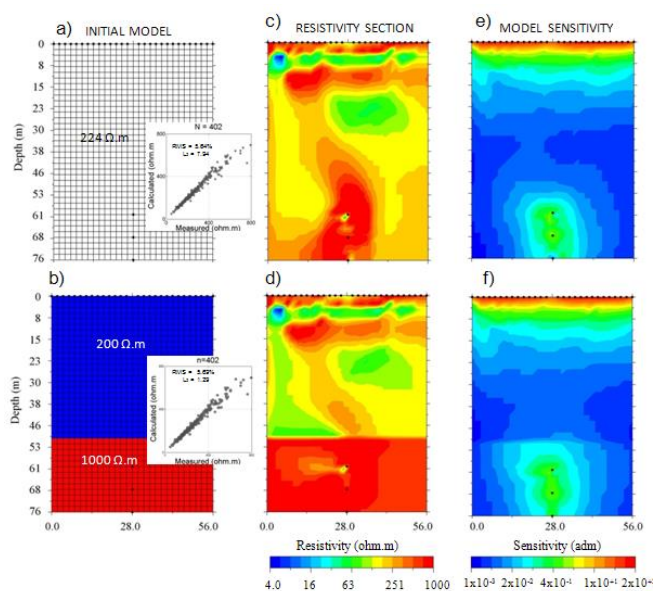
Figure 3: Resistivity sections (c, and d) and respective sensitivity maps (e and f) for a resistivity survey with surface electrode with separation of 2 m (profile length of 54 m). Resistivity sections corresponding to uniform half-space (a) and a two-layers model (b) with insets of cross-plots between measured data and evaluated model response.

For the profile with 108 m, on the other hand, the combination of a larger array length with electrodes in the borehole better distributed the sensitivity. In this case, the intermediary levels are better resolved, outlining the conductivity layer in the corresponding resistivity section. The resistivity model in Figure 4d is then the only one that is compatible with geological information that the conductive layer has lateral continuity. All other models presented a spurious connection between the basement and the upper resistive layers because of lower sensitivity at intermediary levels. The sensitivity analysis allows in addition assessing the vicinity from the electrodes where the resistivity section is recovered by the data. For example, the horizontal continuity of the basement top is retrieved from the data only in a vicinity of the down hole electrodes. The extension of this feature until the limits of the model window lies more on the choice of the reference model than data information itself.

Conclusions

We presented a case study of a surface-down hole ERT survey at a test site (SGTS) of the University of Sao Paulo, Brazil. The resistivity model was able to map variations of a clay unit that could not be sense with only surface electrodes. The use of an appropriate initial model as a reference for the inversion was significant to obtain a reliable model, compatible with previous geological and geophysical information. The model sensitivity map showed that the main geological units imaged were in good agreement with information provided by a well, and the calculated values are therefore reliable. This study also shows the importance of the use of model sensitivity maps when using unconventional array configurations. Our results are useful in illustrating the importance of the array length

when combining surface and down hole electrodes in resistivity imaging. In addition, they show that smaller modifications in the acquisition parameters, in this case increasing from 2 m to 4 m, the separation between the surface electrodes, substantially may improve the resistivity model and its geological interpretation. This result is significant for areas with no free-space for large arrays, such as the city of São Paulo, despite the importance of deeper investigations for subsurface engineering work in the São Paulo Basin.
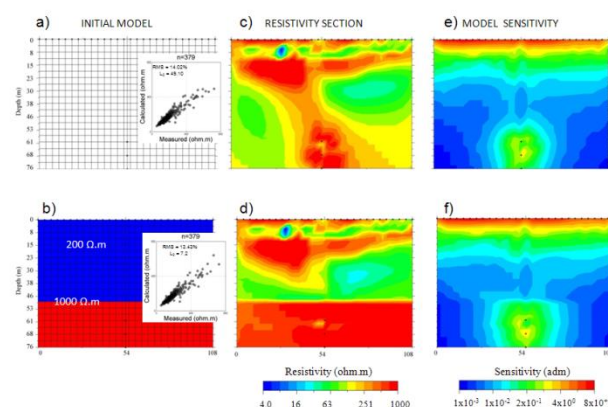

Figure 4: Resistivity sections (c, and d) and respective sensitivity maps (e and f) for a resistivity survey with surface electrode with separation of 4 m (profile length of 108 m). Resistivity sections corresponding to uniform half-space (a) and a two-layers model (b) with insets of cross-plots between measured data and evaluated model response.

References

Bergmann, P., C. Schmidt-Hattenberger, D. Kiessling, C. Rücker, T. Labitzke, J. Henninges, G. Baumann, H. Schütt, 2012, Surface-down hole electrical resistivity tomography applied to monitoring of CO_2 storage at Ketzin, Germany: Geophysics, 77, B253–B267. doi: 10.1190/GEO2011-0515.1

Danielsen, B. E., T. Dahlin, 2010, Numerical modelling of resolution and sensitivity of ERT in horizontal boreholes: Journal of Applied Geophysics, 70, 245–254. doi:10.1016/j.jappgeo.2010.01.005.

Haber, E., U. M. Ascher, D. Oldenburg, 2000, On optimization techniques for solving nonlinear inverse problems: Inverse Problems, 16, 1263–1280. doi:10.1088/0266-5611/16/5/309.

Hansen, P. C., 1992, Analysis of discrete ill-posed problems by means of the L-curve: SIAM Review, 34, 561-580. doi: 10.1137/1034115.

Karaoulis, M., A. Revil, P. Tsourlos, D.D. Werkema, B. J. Minsley, 2013, IP4DI: A software for time-lapse 2D/3D DC-resistivity and induced polarization tomography,

Computers & Geosciences, 54, 164-170. doi:10.1016/j.cageo.2013.01.008.

Loke, M.H., J.E. Chambers, D.F. Rucker, O. Kuras, P.B. Wilkinson, 2013, Recent developments in the direct-current geoelectrical imaging method: Journal of Applied Geophysics, 95, 135-156. doi:10.1016/j.jappgeo.2013.02.017.

Mendonça, C.A., R. Doherty, A. Fornaro, E. L. Abreu, G. C. Novaes, S. Jr. S. Fachin, M. A. La-Scalea, 2015, Integrated earth resistivity tomography (ERT) and multilevel sampling gas: a tool to map geogenic and anthropogenic methane accumulation on brownfield sites: Environ Earth Science. doi:10.1007/s12665-015-4111-6.

Pidlisecky, A., R. Knight, E. Haber, 2006, Cone-based electrical resistivity tomography: Geophysics, 71, G157–G167. doi:10.1190/1.2213205.

Pidlisecky, A., E. Haber, R. Knight, 2007; RESINVM3D: A 3D resistivity inversion package, Geophysics,72, H1-H10. doi:10.1190/1.2402499.

Porsani, J. L., W. R. Borges, V. R., Elis, L. A. Diogo, F. Y. Hiodo,A. Marrano and C. A. Birelli, 2004, Investigações geofísicas de superfície e de poço no sítio controlado de geofísica rasa do IAG-USP. Revista Brasileira de Geofisica:22, 245-258. doi:10.1590/S0102-261X2004000300004.

Power, C., J. I. Gerhard, P. Tsourlos, P. Soupios, K. Simyrdanis, M. Karaoulis, 2015, Improved time-lapse electrical resistivity tomography monitoring of dense non-aqueous phase liquids with surface-to-horizontal borehole arrays: Journal of Applied Geophysics, 112, 1-13. doi:10.1016/j.jappgeo.2014.10.022.

Tsokas, G.N., P.I. Tsourlos, J. Kim, C. B. Papazachos, G. Vargemezis, P. Bogiatzis, 2014, Assessing the condition of the rock mass over the tunnel of Eupalinus in Samos (Greece) using both conventional geophysical methods and surface to tunnel electrical resistivity tomography, Archaeological Prospection, 21, 277-291. doi:10.1002/arp.1489.